Quasi-continuum approximations for travelling kinks in diatomic lattices

2001 J. Phys. A: Math. Gen. 34 7163

(http://iopscience.iop.org/0305-4470/34/36/304)

INSTITUTE OF PHYSICS PUBLISHING JOURNAL OF PHYSICS A: MATHEMATICAL AND GENERAL

J. Phys. A: Math. Gen. **34** (2001) 7163–7180 PII: S0305-4470(01)24763-5

Quasi-continuum approximations for travelling kinks in diatomic lattices

Russell B Tew and Jonathan A D Wattis[1]

Division of Theoretical Mechanics, School of Mathematical Sciences, University of Nottingham, University Park, Nottingham NG7 2RD, UK

E-mail: Jonathan.Wattis@nottingham.ac.uk

Received 3 May 2001, in final form 13 July 2001
Published 31 August 2001
Online at stacks.iop.org/JPhysA/34/7163

Abstract

We extend the quasi-continuum method of approximation to the case of a diatomic lattice. This is illustrated by a lattice in which both small and large atoms interact with first- and second-nearest neighbours. We show that highly accurate quasi-continuum techniques may be generalized to determine the shape of nontopological kinks. Many previous analyses of such systems have found travelling wave solutions only for one particular speed using a second-order continuum theory; we show (i) how wave shapes can be found for arbitrary speeds, and (ii) how solution profiles can be calculated from fourth-order partial differential equations which approximate the lattice. Alongside the theoretical analysis, we also present numerical simulations of the lattice which demonstrate propagation of the predicted waves through the lattice. We show that the particular speed for which solutions have been found in previous studies is a special speed for waves in the lattice, but waves can travel for long periods of time at faster or slower speeds, whilst slowly relaxing to this critical speed.

PACS numbers: 05.45.-a, 05.45.Gg, 05.50.+q

1. Introduction

This paper concerns the approximation of motion of a diatomic lattice using quasi-continuum techniques. The nonlinearity present in such systems allows the existence of solitary waves which are responsible for many important mechanisms in these systems, for example energy localization and transport, and the motion of domain walls through crystal structures. Unfortunately, many previous applications of quasi-continuum techniques have only yielded approximations to solitary waves at one particular speed, since in diatomic lattices the small and large atoms satisfy quite different equations of motion; the only exception we are aware of

[1] Corresponding author.

is that of Henry and Oitmaa [9]. The techniques described in this paper allow these problems to be overcome, and the motions of the sublattices of small and large atoms to be determined for waves travelling at arbitrary speeds.

Many papers have been written about the dynamics of nonlinear lattice problems, for a good review of applications and basic theoretical methods, see Remoissenet [15]. Originally motivated by extensive investigations of Fermi *et al* [8] and Zabusky and Kruskal [22], most concern monatomic lattices. The use of quasi-continuum approximations in lattice problems was initiated by Benjamin *et al* [1], Collins [2–4], and later developed by Rosenau [16], who concentrated on the derivation of well posed partial differential equations as an intermediate stage between the discrete lattice equations and finding the shape of solitary wave solutions. The methods have since been generalized to yield approximations of greater accuracy [6, 17], to multidimensional lattices [7, 19], lattices with second-neighbour interactions (SNIs) [13, 18] and lattices with on-site potentials [20].

Pnevmatikos *et al* [14] investigated the propagation of solitary waves along diatomic chains; considering a model comprising just nonlinear first-neighbour interactions (FNIs), they identified two types of mode: (i) an acoustic mode, in which close neighbours were approximately in phase, and (ii) an optical mode, in which neighbouring atoms oscillated almost exactly out of phase with each other. Their analysis was based on quasi-continuum approximations, which converted the differential-difference equations into a coupled system of two partial differential equations. Numerical simulations of both solution types were performed, revealing small oscillations in the tails of these waves. Their model was extended in [13] to include SNIs, and this model is comparable to the model that we consider. In their papers the continuum equations were simplified using an inspirational, but *ad hoc*, decoupling ansatz, which allowed the form of solitary waves to be found. Again, acoustic and optical modes were identified; along with breather solutions for certain potentials and speeds.

Peyrard *et al* [12] investigated the propagation of solitary waves through a simpler diatomic lattice, where nonlinear FNIs were replaced by linear springs, and an additional 'on-site' nonlinear potential energy was introduced. Despite this simplification, their continuum techniques still yielded a shape only for one particular speed. The propagation of (acoustic) kinks through the lattice was the main theme of the paper. Numerical studies presented solved a forced and damped diatomic lattice, illustrating the pinning of the kink for small values of the forcing parameter. This model was later studied by Cretegny and Peyrard [5], who pointed out deficiencies of quasi-continuum techniques in failing to capture any details on the Peierls–Nabarro barriers. They then used collective coordinates to analyse the effects of discreteness of the underlying lattice structure. Our new quasi-continuum techniques have been tested on this lattice in [21]. Here we shall consider a slightly modified diatomic lattice without forcing or damping, but will find the shape of the travelling solitary waves for general speeds. Henry and Oitmaa [9] studied a similar system, with linear FNIs and an on-site potential for the smaller atoms only. They used a second-order quasi-continuum technique to derive the form of the solution for a variety of wave speeds. Finally we mention that Kofane *et al* [10] study an electrical transmission line which is equivalent to a diatomic mass system with nonlinear FNIs (no SNIs and no on-site potential). They also use continuum approximations and an *ansatz* to separate the two parts of the system and so end up with a solvable equation for the travelling wave. They go on to describe experimental results, wave interactions and recurrence phenomena in the system.

This paper concerns a lattice with a number of complications: SNIs as well as FNIs, the presence of a nonlinear on-site potential and the diatomic nature of the lattice, the final property meaning that there are two displacement variables to find, namely the motion of the sublattices of the larger and the smaller atoms. We shall address these issues by further generalizing

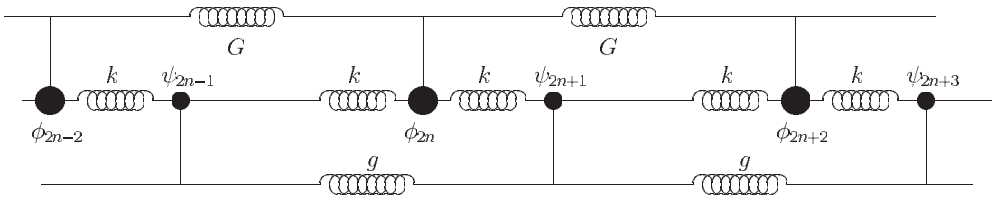

Figure 1. Model system of small and large atoms; interactions with first- and second-nearest neighbours are represented by springs with constants k, g and G.

the method of quasi-continuum approximations. Few papers have addressed the problems of calculating the motion of a diatomic lattice, and those which have highlight limitations of the available techniques. The most notable papers are by Peyrard *et al* [12]. In the next section, we introduce and describe the model, and its basic equilibrium properties. Section 3 deals with the simple second-order continuum theory, which is extended to fourth order in section 4. The discrete system is then simulated numerically in section 5, which is followed by a final section discussing the results of the paper.

2. Model

In this section we introduce the physical system and derive the governing equations. A simple analysis of these equations identifies a combination of parameters with an associated critical value, from which we find two types of equilibrium solution: a symmetric one for strong FNIs, where each small atom is centred between two adjacent large atoms (illustrated in figure 4), and a pair of asymmetric solutions in which each small atom is closely associated with one or other of its neighbouring larger atoms. The latter case supports kink-type travelling wave solutions, which are analysed in later sections of this paper. To be more specific, the lattice under consideration here is composed of two types of atom: a large atom of mass M and a small atom of mass m, with interactions as illustrated in figure 1. It is assumed that the rest of the lattice is close to its minimum-energy configuration; that is, all the large atoms lie in the regular crystal structure and the associated small atoms lie close to the bottom of their potential wells.

The cause of the interactions between first- and second-nearest-neighbour atoms in the lattice is unimportant; they could be ionic or covalent bonds, or van der Waals forces etc. The interactions will be modelled by a system of linear springs. The constants associated with these springs reflect the relative strength of the many interactions each atom has with its neighbours, thus influencing the frequency of small-amplitude disturbances about the atom's equilibrium position. It is assumed that atoms not in the particular chain under consideration influence atoms within the chain through an 'on-site' potential.

The position of each atom in the single chain under consideration will be denoted using the system of variables illustrated in figure 2. The variable $\phi_{2n}(t)$ represents the displacement of the large atom at position n relative to its equilibrium position and $\psi_{2n+1}(t)$ represents the position of its neighbouring small atom relative to the midpoint of $\phi_{2n}(t)$ and $\phi_{2n+2}(t)$ at equilibrium. Note that this means that $\psi_{2n+1} = 0$ does not necessarily represent the equilibrium position of the small atom. For large atoms, this potential is assumed to have a single well; for simplicity we take a quadratic shape, namely $V_H = \sum_n \frac{1}{2} H \phi_{2n}^2$. The on-site potential for a small atom has the form of a double well since small atoms are assumed to closely associate with one of the two neighbouring large atoms. The simplest function having such a shape is a

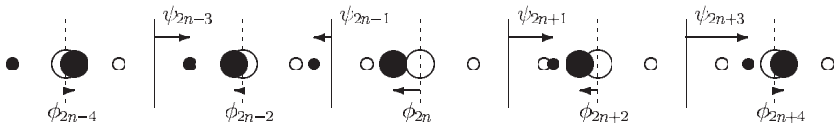

Figure 2. Notation for the displacements of the atoms from equilibrium. The displacements of the large atoms are denoted by ϕ_{2n}, which is measured from their equilibrium positions (the dotted lines). The displacements of the smaller atoms are measured from the midpoints of the equilibria of large atoms (the solid lines). In this figure $\phi_{2n+2} < 0$, $\phi_{2n+4} > 0$, $\psi_{2n-1} < 0$ and $\psi_{2n+1} > 0$.

quartic, namely $V_h = \sum_n \frac{1}{4}h(\psi_{2n+1}^2 - \overline{\psi}^2)^2$. The Hamiltonian of the system is thus

$$\mathcal{H} = \sum_n \left\{ \tfrac{1}{2}M\dot{\phi}_{2n}^2 + \tfrac{1}{2}m\dot{\psi}_{2n+1}^2 + \tfrac{1}{2}k(\phi_{2n} - \psi_{2n+1})^2 + \tfrac{1}{2}k(\phi_{2n} - \psi_{2n-1})^2 + \tfrac{1}{2}G(\phi_{2n} - \phi_{2n+2})^2 \right.$$
$$\left. + \tfrac{1}{2}g(\psi_{2n+1} - \psi_{2n-1})^2 + \tfrac{1}{2}H\phi_{2n}^2 + \tfrac{1}{4}h(\psi_{2n+1}^2 - \overline{\psi}^2)^2 \right\}. \tag{2.1}$$

2.1. Minimum-energy configuration

The system is in its most stable (lowest-energy) state when all of the small atoms in the chain are in the same energy well (either the left or right). Other stationary states are possible, and will be investigated later. One example is that in the left part of the chain all the small atoms are to the left of the closest large atom. In the right part of the chain they lie to the right side; in between these two limits there is a transition region, where atoms lie between the two extremal cases. In this example there is a deficit of small atoms over large atoms in the transition region. Conversely the case can occur when in the left part of the chain all of the small atoms lie to the right side of the closest large atom, and in the right part they lie to the left of the closest large atom. In this case there is a surplus of small atoms over large atoms in the transition region. These are illustrated in figure 5.

Before we consider these more complex stationary solutions and the motion of such transition regions, let us consider the details of the minimum-energy configuration of (2.1). At minimum energy it is assumed that there is no particle motion, and all large atoms have the same displacement from equilibrium, so that there is no energy due to SNIs. We make a similar assumption for the small atoms so that

$$\phi_{2n}(t) = \phi \qquad \text{and} \qquad \psi_{2n+1}(t) = \psi. \tag{2.2}$$

The potential energy is then a sum over identical and repeating cells. For each cell the energy is

$$\mathcal{V}_{\text{cell}} = k(\phi - \psi)^2 + \tfrac{1}{2}H\phi^2 + \tfrac{1}{4}h(\psi^2 - \overline{\psi}^2)^2 \tag{2.3}$$

which we think of as the energy density of the system. Minimizing this with respect to ψ and ϕ leads to

$$0 = 2k(\phi - \psi) - h\psi(\psi^2 - \overline{\psi}^2) \qquad 0 = 2k(\phi - \psi) + H\phi \tag{2.4}$$

the latter of which is solved by

$$\phi = \frac{2k}{2k + H}\psi. \tag{2.5}$$

Substituting (2.5) into (2.4) yields $\psi = 0$ or

$$\psi^2 = \tilde{\psi}^2 := \frac{Hh\overline{\psi}^2 + 2k(h\overline{\psi}^2 - H)}{h(H + 2k)}. \tag{2.6}$$

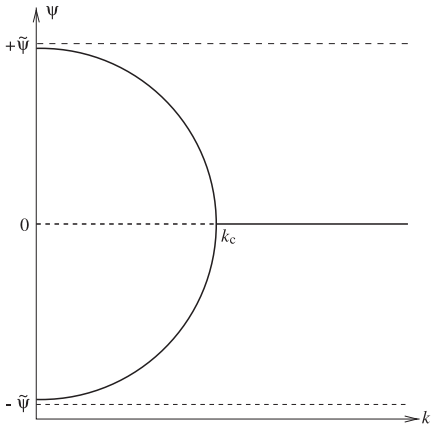

Figure 3. Bifurcation diagram, showing that for $k > k_c$ there is only the trivial stationary solution, but that for $k < k_c$ there are three stationary solutions, the zero solution being unstable and the two nonzero solutions ($\psi = \pm\tilde{\psi}$) being stable.

Figure 4. Illustration of the symmetric arrangement of smaller atoms which is the only stationary solution when $k > k_c$, where it is stable. This is also an unstable solution in the case $k < k_c$.

For $\tilde{\psi}$ to be real, we require $H(h\overline{\psi}^2 - 2k) + 2kh\overline{\psi}^2 > 0$, thus the nonzero solution for ψ can only exist if $k < k_c$ where

$$k_c = \frac{Hh\overline{\psi}^2}{2(H - h\overline{\psi}^2)}. \tag{2.7}$$

Figure 3 illustrates the stability of the system as a bifurcation diagram. For $k > k_c$ we can see that the only solution is $\psi = 0$, which from (2.5) corresponds to $\phi = 0$. Substitution of $\phi = 0 = \psi$ into (2.3) yields the energy $\mathcal{V}_{\text{cell}} = \frac{1}{4}h\overline{\psi}^4$. This solution is stable, since an expansion of $\mathcal{V}_{\text{cell}}$ for small (ψ, ϕ) shows $(0, 0)$ to be a minimum. The configuration of small and large atoms in this case is illustrated in figure 4. When $k < k_c$ three solutions exist; one solution is the zero solution described above. However, this solution is now unstable, since $\psi = 0$, $\phi = 0$ is now a saddle point of $\mathcal{V}_{\text{cell}}$. The other solutions, $\psi = \pm\tilde{\psi}$ with $\phi = \tilde{\phi} := 2k\tilde{\psi}/(2k + H)$, are stable, being minima of $\mathcal{V}_{\text{cell}}$. Note that at minimum total energy the small atom does not lie at the bottom of the on-site potential well ($\overline{\psi}$ of V_h), due to the competing effect of the FNIs.

2.2. Equations of motion

From (2.1) we obtain the equations of motion

$$m\ddot{\psi}_{2n+1} = k(\phi_{2n+2} - 2\psi_{2n+1} + \phi_{2n-2}) + g(\psi_{2n+3} - 2\psi_{2n+1} + \psi_{2n-1}) - h\psi_{2n+1}(\psi_{2n+1}^2 - \overline{\psi}^2) \tag{2.8}$$

$$M\ddot{\phi}_{2n} = k(\psi_{2n+1} - 2\phi_{2n} + \psi_{2n-1}) + G(\phi_{2n+2} - 2\phi_{2n} + \phi_{2n-2}) - H\phi_{2n} \tag{2.9}$$

which describe the motion of the small and large atoms of the lattice respectively. The response to small-amplitude disturbances can be determined from the system linearized about the zero solution, by assuming $\phi_{2n}(t) \sim \tilde{\phi} + \hat{\phi}\,\mathrm{e}^{\mathrm{i}\omega t + 2n\mathrm{i}p}$ and $\psi_{2n+1}(t) \sim \tilde{\psi} + \hat{\psi}\,\mathrm{e}^{\mathrm{i}\omega t + (2n+1)\mathrm{i}p}$ with $\hat{\phi}$, $\hat{\psi} \ll 1$. This yields the dispersion relation, $\omega = \omega(p)$ for wavenumber p, for the system (2.8), (2.9) as

$$\begin{aligned} 0 = {} & Mm\omega^4 - (mH + 2km + 2kM + 2Mh\tilde{\psi}^2 + 4gM\sin^2 p + 4Gm\sin^2 p)\omega^2 \\ & + (2h\overline{\psi}^2 + 2k + 4g\sin^2 p)(H + 2k + 4G\sin^2 p) - 4k^2\cos^2 p. \end{aligned} \tag{2.10}$$

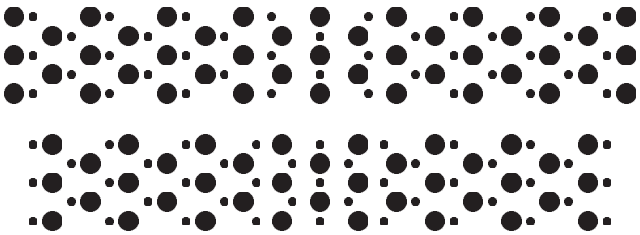

Figure 5. Illustration of domain walls in a two-dimensional layer of a crystal. Atoms on the left are in one minimum-energy configuration and the atoms on the right are in a different minimum-energy configuration. Across the atoms in the centre of the figure there is a gradual transition from one equilibrium state to the other.

Small disturbances about homogeneous solutions of the equations only determine the stability of such states. We are concerned with the dynamics associated with larger-scale structure, such as domain walls, as illustrated in figure 5. This figure illustrates the two situations in which one equilibrium solution is approached in the limit $n \to -\infty$, and the other equilibrium solution in the limit $n \to +\infty$.

3. Simple continuum theory

In this section we describe the reduction of the system of coupled differential-difference equations (2.8) and (2.9) to a coupled pair of second-order partial differential equations, which allow further analysis. We then seek travelling kink solutions to the resulting nonlinear equations.

We begin by replacing the discrete variable, n, by a continuous counterpart, x, in (2.8), (2.9). Taylor expansions then allow the original system to be rewritten as partial differential equations. Thus we replace $\phi_{n+2}(t)$ by $\phi(x,t) + 2\phi_x(x,t) + 2\phi_{xx}(x,t)$, with similar expressions holding for $\phi_{n\pm1}$, $\psi_{n\pm1}$ etc. We expand (2.9) around $x = 2n$ and (2.8) around $x = 2n+1$, which yields

$$m\psi_{tt} = 4g\psi_{xx} + k\phi_{xx} - (h\overline{\psi}^2 - 2k)\psi + 2k\phi - h\psi^3 \tag{3.1}$$

$$M\phi_{tt} = 4G\phi_{xx} + k\psi_{xx} - (H + 2k)\phi + 2k\psi \tag{3.2}$$

where derivatives are denoted by subscripts. Fourth- and higher-order derivatives are neglected since $\phi(x,t)$ and $\psi(x,t)$ are assumed to be slowly varying in space.

Equations (3.1), (3.2) contain the eight original physical parameters, which can be reduced by nondimensionalizing the system: using $\phi = \Phi_0\Phi$, $\psi = \Psi_0\Psi$, $t = T_0T$ and $x = X_0X$, we find

$$\Psi_{TT} = \Psi_{XX} + \Phi_{XX} + \alpha\Phi + \Psi - \Psi^3 \tag{3.3}$$

$$\Phi_{TT} = \beta\Phi_{XX} + \gamma\Psi_{XX} + \alpha\gamma\Psi - \varepsilon\Phi \tag{3.4}$$

where

$$\begin{aligned} \Phi_0 &= \frac{4g}{k}\sqrt{\frac{h\overline{\psi}^2 - 2k}{h}} \qquad & \Psi_0 &= \sqrt{\frac{h\overline{\psi}^2 - 2k}{h}} \\ X_0 &= 2\sqrt{\frac{g}{h\overline{\psi}^2 - 2k}} \qquad & T_0 &= \sqrt{\frac{m}{h\overline{\psi}^2 - 2k}} \end{aligned} \tag{3.5}$$

and

$$\alpha = \frac{8g}{h\overline{\psi}^2 - 2k} \qquad \beta = \frac{Gm}{gM} \qquad \gamma = \frac{k^2 m}{16g^2 M} \qquad \varepsilon = \frac{m(2k+H)}{M(h\overline{\psi}^2 - 2k)}. \tag{3.6}$$

Here we are interested in the situation in which the on-site potential is strong enough to cause the small atoms to be closer to one neighbouring larger atom than the other at equilibrium. Thus we assume $h\overline{\psi}^2 - 2k > 0$. In these nondimensional variables the minimum-energy configurations (2.5), (2.6) correspond to

$$\Psi = \pm\tilde{\Psi} = \pm\sqrt{1 + \frac{\gamma\alpha^2}{\varepsilon}} \qquad \Phi = \frac{\gamma\alpha\tilde{\Psi}}{\varepsilon}. \tag{3.7}$$

The existence of $\tilde{\Psi}$ requires the inequality $\gamma\alpha^2/\varepsilon > -1$ to be satisfied.

3.1. Solitary wave solution for special speed

In this subsection we briefly recap the existing continuum theory for diatomic lattices, before generalizing the theory to arbitrary speeds in the next subsection. For the nonlinear problem we search for travelling-wave solutions. Substitution of $\Phi(X, T) = \Phi(X - cT) = \Phi(Z)$ and $\Psi(X, T) = \Psi(X - cT) = \Psi(Z)$ into (3.3) and (3.4) yields

$$(c^2 - 1)\Psi'' = \Phi'' + \alpha\Phi + \Psi - \Psi^3 \tag{3.8}$$

$$(c^2 - \beta)\Phi'' = \gamma\Psi'' + \alpha\gamma\Psi - \varepsilon\Phi. \tag{3.9}$$

Similar equations to these were obtained by Cretegny and Peyrard [5] and Peyrard *et al* [12], who proceeded to consider the special speed $c_* = \sqrt{\beta}$, which reduces (3.9) to an algebraic equation for $\Phi(Z)$

$$\Phi = \frac{\gamma}{\varepsilon}\Psi'' + \frac{\alpha\gamma}{\varepsilon}\Psi. \tag{3.10}$$

This implies $\Phi'' = \alpha\gamma\Psi''/\varepsilon$ since, in order to be consistent with the approximations we have already made, fourth derivatives are ignored. Substituting these expressions into (3.8) yields a second-order nonlinear ordinary differential equation for $\Psi(Z)$

$$0 = \left(\beta - 1 - \frac{2\alpha\gamma}{\varepsilon}\right)\Psi'' - \left(\frac{\alpha^2\gamma}{\varepsilon} + 1\right)\Psi + \Psi^3. \tag{3.11}$$

The first integral of this is

$$E = \frac{1}{2}\left(1 + \frac{2\alpha\gamma}{\varepsilon} - \beta\right)(\Psi')^2 + \frac{1}{2}\left(1 + \frac{\alpha\gamma}{\varepsilon}\right)\Psi^2 - \frac{1}{4}\Psi^4 \tag{3.12}$$

in which E can be thought of as an energy. A plot of E against Ψ, Ψ' appears qualitatively like that displayed in figure 6. Level curves of the surface represent trajectories in (Ψ, Ψ') phase space. Placed symmetrically either side of the minimum are two saddle points, which represent the equilibrium values $(\Psi = \pm\tilde{\Psi}, \Psi' = 0)$ joined by the homoclinic trajectory.

By imposing the boundary conditions $\Psi \to \tilde{\Psi}$ and $\Psi' \to 0$ as $Z \to +\infty$, we find the value of E corresponding to the homoclinic connection, namely $E = \frac{1}{4}\tilde{\Psi}^4$; this enables (3.12) to be integrated. We thus find

$$\Psi(Z) = \pm\tilde{\Psi}\tanh(\theta(Z - Z_0)) \qquad \text{where} \quad \theta = \frac{1}{2}\sqrt{\frac{\varepsilon + \gamma\alpha^2}{2\alpha\gamma + \varepsilon - \beta\varepsilon}} \tag{3.13}$$

and Z_0 is a constant of integration which determines the phase of the wave. Substitution of $\Psi(Z)$ from (3.13) and its derivatives into (3.10) yields $\Phi(Z)$

$$\Phi(Z) = \frac{\pm\alpha\gamma\tilde{\Psi}}{\varepsilon}\tanh(\theta(Z - Z_0))\left(1 - \frac{2\theta^2}{\alpha}\operatorname{sech}^2(\theta(Z - Z_0))\right). \tag{3.14}$$

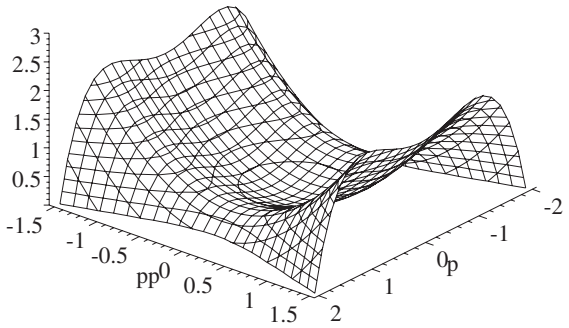

Figure 6. A plot of the quantity E defined in (3.12) against $p = \Psi$ and $pp = \Psi'$, for the case $\alpha = 0.25$, $\beta = 1$, $\gamma = 1.4$, $\varepsilon = 1$, $c = 0.5$.

3.2. Solitary wave solution for general speed

At this point it should be remembered that the analysis of the travelling wave solution of (3.8), (3.9) so far presented in this section has been for the special speed $c = c_* = \sqrt{\beta}$, which greatly simplifies equation (3.9). We now investigate solitary waves for general speeds.

As with the previous analysis we will begin by using (3.9) to eliminate Φ. Rewriting (3.9) as

$$\varepsilon\left(1 + \frac{c^2 - \beta}{\varepsilon}\frac{\mathrm{d}^2}{\mathrm{d}Z^2}\right)\Phi(z) = \alpha\gamma\left(1 + \frac{1}{\alpha}\frac{\mathrm{d}^2}{\mathrm{d}Z^2}\right)\Psi(Z) \tag{3.15}$$

and noting that $c^2 \neq \beta$, we invert the operator on the left-hand side, using the fact that to second order $(1 + K\frac{\mathrm{d}^2}{\mathrm{d}Z^2})^{-1} = 1 - K\frac{\mathrm{d}^2}{\mathrm{d}Z^2}$. Applying such an inverse operator to both sides of (3.15) and neglecting fourth-order derivatives we obtain

$$\Phi(Z) = \frac{\gamma\alpha}{\varepsilon}\left(\Psi(Z) + \left(\frac{\alpha\beta + \varepsilon - \alpha c^2}{\alpha\varepsilon}\right)\Psi''(Z)\right) \tag{3.16}$$

in place of (3.10) (though note that this reduces to (3.10) in the case $c = c_* = \sqrt{\beta}$). Substitution of this expression along with its derivatives ($\Phi'' = \gamma\alpha\Psi''/\varepsilon$ since we neglect fourth-derivative terms) into (3.8) yields

$$\left(\frac{(\varepsilon^2 + 2\gamma\alpha\varepsilon + \gamma\beta\alpha^2) - c^2(\varepsilon^2 + \alpha^2\gamma)}{\varepsilon^2}\right)\Psi'' + \left(\frac{\alpha^2\gamma + \varepsilon}{\varepsilon}\right)\Psi - \Psi^3 = 0 \tag{3.17}$$

which can be integrated to

$$E = \frac{1}{2}\left(\frac{(\varepsilon^2 + 2\gamma\alpha\varepsilon + \gamma\beta\alpha^2) - c^2(\varepsilon^2 + \alpha^2\gamma)}{\varepsilon^2}\right)(\Psi')^2 + \frac{1}{2}\left(1 + \frac{\gamma\alpha^2}{\varepsilon}\right)\Psi^2 - \frac{1}{4}\Psi^4. \tag{3.18}$$

The surface $E = E(\Psi, \Psi')$ is shown in figure 6 for the case in which the coefficient of $(\Psi')^2$ is positive. Level curves of this surface correspond to trajectories of the system in (Ψ, Ψ') phase space. For there to be a trajectory joining the two equilibrium points, that is the saddle point at $(\Psi = \tilde{\Psi}, \Psi = 0)$ to the other saddle point at $(\Psi = -\tilde{\Psi}, \Psi = 0)$, we require the coefficient of $(\Psi')^2$ to be positive. This condition imposes a maximum speed on the system, above which kink solutions of (3.17) do not exist: this speed is given by

$$c_{\max} = \sqrt{\frac{\varepsilon^2 + 2\gamma\alpha\varepsilon + \alpha^2\beta\gamma}{\varepsilon^2 + \gamma\alpha^2}}. \tag{3.19}$$

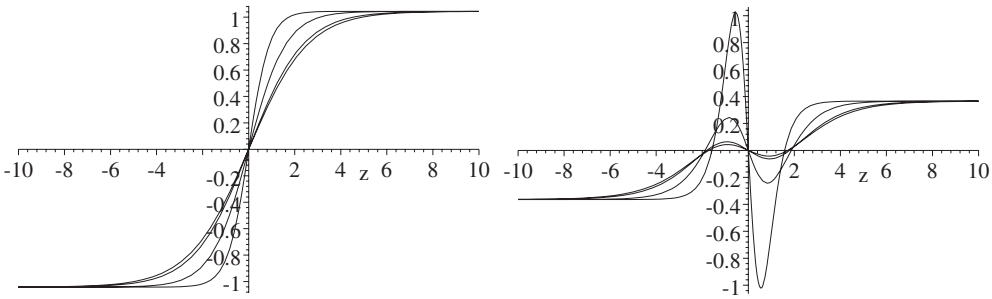

Figure 7. The second-order approximation to the travelling wave; $\Psi(Z)$ above, and $\Phi(Z)$ below, in the case $\alpha = 0.25$, $\beta = 1.0$, $\gamma = 1.4$, $\varepsilon = 1.0$, for the speeds $c = 0$, 0.5, 1.0, 1.2. Faster speeds correspond to steeper gradients in the plot of $\Psi(Z)$, and larger-amplitude oscillations in $\Phi(Z)$ near the origin.

Above this speed the equilibrium points $(\Psi, \Psi') = (\pm\tilde{\Psi}, 0)$ are transformed from saddle points (as illustrated in figure 6) to maxima, consequently the trajectory joining them is destroyed.

Returning to (3.18) in the case $c < c_{\max}$, we insert the boundary conditions $\Psi \to \tilde{\Psi}$, $\Psi' \to 0$ as $Z \to +\infty$ to find the constant E as $E = \frac{1}{4}\tilde{\Psi}^2$. Equation (3.18) can then be integrated to find the solution

$$\Psi(Z) = \tilde{\Psi}\ \tanh(\theta(Z - Z_0)) \qquad \text{where} \quad \theta = \frac{1}{2}\sqrt{\frac{\varepsilon(\varepsilon + \gamma\alpha^2)}{(\varepsilon^2 + 2\alpha\gamma\varepsilon + \alpha^2\beta\gamma) - c^2(\varepsilon^2 + \gamma\alpha^2)}}. \tag{3.20}$$

Substitution of this solution into (3.16) yields

$$\Phi(Z) = \frac{\gamma\alpha}{\varepsilon}\ \tanh(\theta(Z - Z_0))\left(1 - \frac{2\theta^2}{\varepsilon\alpha}(\alpha\beta + \varepsilon - \alpha c^2)\operatorname{sech}^2(\theta(Z - Z_0))\right). \tag{3.21}$$

The shapes of these waves are illustrated in figure 7.

Notice that the oscillations near the origin of the graph of $\Phi(Z)$ increase in size with increasing speed, but do not disappear in the limit of small speed; figure 7 shows the curves for $c = 0$ and 0.5 being almost coincident. For the parameter values used in figure 7, the maximum speed is $c_{\max} = 1.282$. Note also that faster waves have reduced width in $\Psi(Z)$. This is not so apparent in $\Phi(Z)$ due to the above-mentioned oscillations, but is manifest in the more rapid decay to equilibrium at large values of $|Z|$.

4. Fourth-order quasi-continuum theory

In this section we extend the quasi-continuum approximation used in section 3, by incorporating fourth-order derivatives from the Taylor series expansions of the difference terms as well as the second-order derivatives already included. Thus we expect the results of this section to be more accurate than those of section 3, at the expense of greater complication.

A fourth-order expansion of (2.8) and (2.9) yields the two coupled fourth-order partial differential equations

$$m\psi_{tt} = \tfrac{4}{3}g\psi_{xxxx} + \tfrac{1}{12}k\phi_{xxxx} + 4g\psi_{xx} + k\phi_{xx} - (h\overline{\psi}^2 - 2k)\psi + 2k\phi - h\psi^3 \tag{4.1}$$

$$M\phi_{tt} = \tfrac{4}{3}G\phi_{xxxx} + \tfrac{1}{12}k\psi_{xxxx} + 4G\phi_{xx} + k\psi_{xx} - (H + 2k)\phi + 2k\psi. \tag{4.2}$$

Applying the same nondimensionalization as in (3.5) and (3.6), we find the dimensionless equations

$$\Psi_{TT} = \frac{2}{3\alpha}\Psi_{XXXX} + \frac{1}{6\alpha}\Phi_{XXXX} + \Psi_{XX} + \Phi_{XX} + \Psi + \alpha\Phi - \Psi^3 \tag{4.3}$$

$$\Phi_{TT} = \frac{2\beta}{3\alpha}\Phi_{XXXX} + \frac{\gamma}{6\alpha}\Psi_{XXXX} + \beta\Phi_{XX} + \gamma\Psi_{XX} - \varepsilon\Phi + \alpha\gamma\Psi. \tag{4.4}$$

To search for a travelling-wave solution we substitute $\Phi(X, T) = \Phi(X - cT) = \Phi(Z)$ and $\Psi(X, T) = \Psi(X - cT) = \Psi(Z)$ into (4.3) and (4.4), yielding

$$0 = \frac{2}{3\alpha}\Psi'''' + \frac{1}{6\alpha}\Phi'''' + (1 - c^2)\Psi'' + \Phi'' - \Psi + \alpha\Phi - \Psi^3 \tag{4.5}$$

$$0 = \frac{2\beta}{3\alpha}\Phi'''' + \frac{\gamma}{6\alpha}\Psi'''' + (\beta - c^2)\Phi'' + \gamma\Psi'' - \varepsilon\Phi + \alpha\gamma\Psi. \tag{4.6}$$

The latter equation (4.6) is used to eliminate $\Phi(Z)$ from the former (4.5). We rewrite (4.6) as

$$\varepsilon\left(1 - \frac{(\beta - c^2)}{\varepsilon}\frac{\mathrm{d}^2}{\mathrm{d}Z^2} - \frac{2\beta}{3\alpha\varepsilon}\frac{\mathrm{d}^4}{\mathrm{d}Z^4}\right)\Phi(Z) = \gamma\alpha\left(1 + \frac{1}{\alpha}\frac{\mathrm{d}^2}{\mathrm{d}Z^2} + \frac{1}{6\alpha^2}\frac{\mathrm{d}^4}{\mathrm{d}Z^4}\right)\Psi(Z). \tag{4.7}$$

The operator which acts on the left-hand side can be inverted to fourth order to yield the approximation

$$\Phi(Z) = \frac{\gamma\alpha}{\varepsilon}\left[1 + \left(\frac{\varepsilon + \alpha\beta - \alpha c^2}{\alpha\varepsilon}\right)\frac{\mathrm{d}^2}{\mathrm{d}Z^2} + \left(\frac{\varepsilon^2 + 6\alpha\varepsilon(\beta - c^2) + 6\alpha^2(\beta - c^2)^2}{6\alpha^2\varepsilon^2}\right)\frac{\mathrm{d}^4}{\mathrm{d}Z^4}\right]\Psi(Z). \tag{4.8}$$

This formula, together with its second and fourth derivatives can be inserted into (4.5) to obtain

$$\Psi^3 = Q_4\Psi'''' + Q_2\Psi'' + \tilde{\Psi}^2\Psi \tag{4.9}$$

where

$$\begin{aligned} Q_2 &= \frac{1}{\varepsilon^2}\left((\varepsilon^2 + 2\alpha\gamma\varepsilon + \alpha^2\beta\gamma) - (\varepsilon^2 + \alpha^2\gamma)c^2\right) \\ Q_4 &= \frac{2}{3\alpha} + \frac{\gamma}{3\varepsilon^3}\left(\varepsilon(\varepsilon + 2\alpha\beta) + 3(\varepsilon + \alpha\beta - \alpha c^2)^2\right). \end{aligned} \tag{4.10}$$

Approximating the fourth-order derivative operator by a (2,2) Padé approximant we find

$$\Psi^3 = \left(Q_2 - Q_4\frac{\mathrm{d}^2}{\mathrm{d}Z^2}\right)^{-1}\left(Q_2\tilde{\Psi}^2 + (Q_2^2 - Q_4\tilde{\Psi}^2)\frac{\mathrm{d}^2}{\mathrm{d}Z^2}\right)\Psi \tag{4.11}$$

which, on rearranging, yields the second-order nonlinear ordinary differential equation

$$Q_2\Psi^3 - Q_2\tilde{\Psi}^2\Psi = \frac{\mathrm{d}^2}{\mathrm{d}Z^2}\left(Q_4\Psi^3 + (Q_2^2 - Q_4\tilde{\Psi}^2)\Psi\right). \tag{4.12}$$

Although this approximation has more nonlinear terms than were present in (4.9), it has reduced the order of the equation, whilst retaining the fourth-order accuracy. Equation (4.12) can be integrated further, by multiplying through by $(3Q_4\Psi^2 + Q_2^2 - Q_4\tilde{\Psi}^2)\Psi'$ to obtain

$$\begin{aligned} E = {} & \tfrac{1}{2}(\Psi')^2(3Q_4\Psi^2 + Q_2^2 - Q_4\tilde{\Psi}^2)^2 + \tfrac{1}{2}\tilde{\Psi}^2Q_2(Q_2^2 - Q_4\tilde{\Psi}^2)\Psi^2 \\ & + \tfrac{1}{4}Q_2(4Q_4\tilde{\Psi}^2 - Q_2^2)\Psi^4 - \tfrac{1}{2}Q_2Q_4\Psi^6. \end{aligned} \tag{4.13}$$

Applying the boundary conditions $\Psi \to \tilde{\Psi}$, $\Psi' \to 0$ as $Z \to \infty$ yields the constant of integration E as $E = \frac{1}{4}Q_2^3\tilde{\Psi}^4$, allowing the rearrangement of (4.13) to

$$\begin{aligned} & \left[3Q_4\Psi^2 + Q_2^2 - Q_4\tilde{\Psi}^2\right]^2\left(\frac{\mathrm{d}\Psi}{\mathrm{d}z}\right)^2 \\ & \quad = Q_2(\tilde{\Psi}^2 - \Psi^2)\left[\tfrac{1}{2}Q_2^2\tilde{\Psi}^2 - \tfrac{1}{2}(Q_2^2 + Q_4\tilde{\Psi}^2)\Psi^2 - Q_4\Psi^4\right]. \end{aligned} \tag{4.14}$$

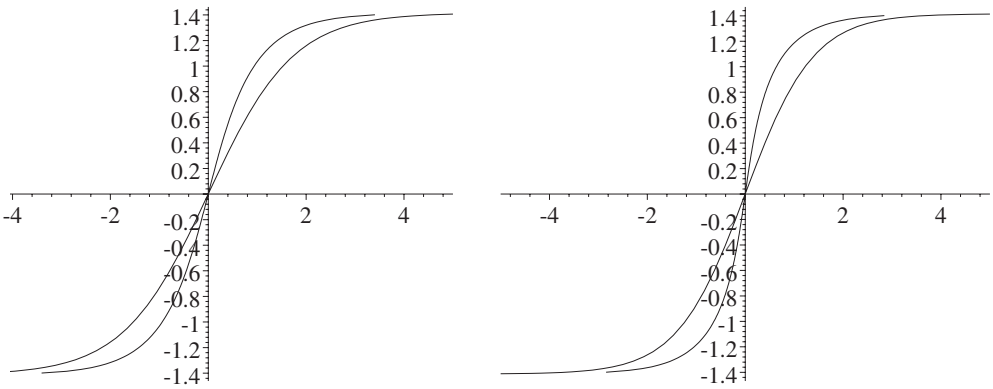

Figure 8. The travelling wave solution in the sublattice of smaller atoms. Ψ is plotted against $Z(\Psi)$ from (4.15) with dimensionless speed $c = 0$ on the left and $c = 0.7$ on the right. In each case the second-order approximation is also displayed for comparison; in both cases the fourth-order solution has the steeper gradient at the origin. The plots are for $\alpha = 10$, $\beta = 3$, $\gamma = 0.1$, $\varepsilon = 10$.

Being separable, this can be integrated to give the implicit solution

$$Z(\Psi) = \int_0^{\Psi} \frac{2(3Q_4u^2 + Q_2^2 - Q_4\tilde{\Psi}^2)\,\mathrm{d}u}{\sqrt{2Q_2(\tilde{\Psi}^2 - u^2)[Q_2^2\tilde{\Psi}^2 - (Q_4\tilde{\Psi}^2 + Q_2^2)u^2 - 2Q_4u^4]}} \tag{4.15}$$

which is illustrated in figure 8.

The form of (4.14) suggests that kink-type solutions exist, Ψ' having zeros at $\Psi = \tilde{\Psi}$ with $\tilde{\Psi}$ defined in exactly the same way as in the second-order analysis (3.7). The terms in square brackets in (4.14) generate a change in shape over the second-order tanh form (3.20). A measure of the width of the solution is given by the reciprocal of the gradient of the kink at $Z = 0$ (that is $1/\Psi'(0)$); from (4.14) we have

$$\Psi'(0) = \frac{\tilde{\Psi}^2 Q_2^{3/2}}{\sqrt{2}\,(Q_2^2 - Q_4\tilde{\Psi}^2)} \tag{4.16}$$

whereas in the second-order theory we have, from (3.18), $\Psi'(0) = \tilde{\Psi}^2/\sqrt{2Q_2}$. Thus the presence of $Q_4 > 0$ increases the gradient of the kink.

Equation (4.15) gives the implicit solution $Z(\Psi)$ rather than $\Psi(Z)$ so finding Φ using (4.8) is not trivial. We construct a parametric form $\Phi(\Psi)$ noting that $\frac{\mathrm{d}}{\mathrm{d}Z} = (1/Z'(\Psi))\frac{\mathrm{d}}{\mathrm{d}\Psi}$, so that

$$\frac{\mathrm{d}\Psi}{\mathrm{d}Z} = \frac{1}{Z'(\Psi)} \qquad \frac{\mathrm{d}^2\Psi}{\mathrm{d}Z^2} = -\frac{Z''(\Psi)}{Z'(\Psi)^3} \qquad \frac{\mathrm{d}^3\Psi}{\mathrm{d}Z^3} = \frac{3Z''(\Psi)^2 - Z'(\Psi)Z'''(\Psi)}{Z'(\Psi)^5} \tag{4.17}$$

$$\frac{\mathrm{d}^4\Psi}{\mathrm{d}Z^4} = \frac{10Z'(\Psi)Z''(\Psi)Z'''(\Psi) - Z'(\Psi)^2Z''''(\Psi) - 15Z''(\Psi)^3}{Z'(\Psi)^7}. \tag{4.18}$$

These enable (4.8) to be used to produce plots of $\Phi(\Psi)$ against $Z(\Psi)$ as illustrated in figure 9. For the choice of parameters used here, the second-order approximation to $\Psi(Z)$ does not have any oscillations; whereas the fourth-order accurate approximation does. This in contrast with figure 7, where the second-order approximation undergoes a limited oscillation, having two stationary points, whereas the oscillations of the fourth-order solution displayed in figure 9 have four stationary points.

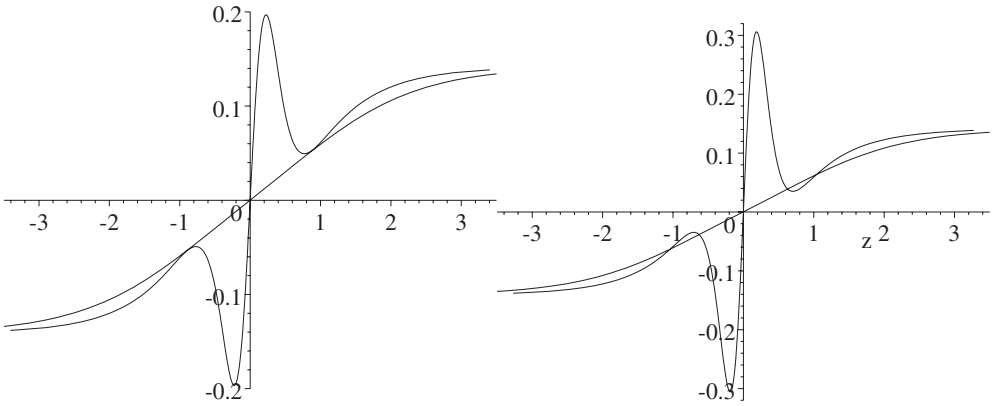

Figure 9. The travelling wave solution in the sublattice of larger atoms. $\Phi(\Psi)$ from (4.8) is plotted against $Z(\Psi)$ from (4.15), using (4.17) and (4.18); on the left for speed $c = 0$, and on the right for $c = 0.35$, in both cases for $\alpha = 10$, $\beta = 3$, $\gamma = 0.1$, $\varepsilon = 10$. The fourth-order approximation includes oscillations, which increase in amplitude with increasing speed.

5. Numerical results

Numerical simulations of the system (2.8) and (2.9) have been carried out using a fourth-order Runge–Kutta scheme coded in Fortran90 with double-precision real variables. The program solves the equations of motion for N atoms where N is even. Initial conditions are taken from the second-order quasi-continuum solution (3.20), (3.21). We implement the boundary conditions by introducing fictitious points at $n = 0, -1$ and $n = N + 1, N + 2$ so that $\psi_1, \phi_2, \psi_{N-1}$ and ϕ_N all have first and second neighbours. We then assume periodic boundary conditions, so that at the ends of the lattice we have

$$\begin{aligned} \psi_{-1} &= \psi_{N-1} - 2\tilde{\psi} & \psi_{N+1} &= \psi_1 + 2\tilde{\psi} \\ \phi_0 &= \phi_N - 2\tilde{\phi} & \phi_{N+2} &= \phi_2 + 2\tilde{\phi} \\ \dot{\psi}_{-1} &= \dot{\psi}_{N-1} & \dot{\psi}_{N+1} &= \dot{\psi}_1 \\ \dot{\phi}_0 &= \dot{\phi}_N & \dot{\phi}_{N+2} &= \dot{\phi}_2 \end{aligned} \tag{5.1}$$

where $2\tilde{\psi}$ is the amplitude of the kink in the sublattice of the smaller atoms and $2\tilde{\phi}$ is the amplitude of the kink in the sublattice of larger atoms. The parameter values used in this section are $G = 14.11$, $g = 14.10$, $M = 16.00$, $m = 8.00$, $H = 10.00$, $h = 18.00$, $k = 1.00$, $\overline{\psi} = 0.51$. Various values for the timestep were tested, and all below $\mathrm{d}t = 0.01$ gave the same results so subsequent simulations were performed with this timestep.

5.1. Propagation through the lattice

Numerical simulations can be used to verify the predicted speed of a wave as it propagates through the lattice. By launching the wave at a variety of speeds, and examining the speed of the wave during and at the end of the simulation, we can gauge the accuracy of our initial condition and evaluate the mobility of the wave as it propagates through the lattice. Results indicating the initial and final speeds of the wave are shown in table 1. In each simulation the wave was initially launched from lattice site $n = 100$ in the direction of larger n, on a lattice of size $N = 5000$ atoms. The simulation was carried out over a time interval of $0 < t < 280$ or until the wave reached a position 100 sites from the end of the lattice (i.e. $n = 4900$). The speed was measured as an average over a time interval of length 21. An illustration of the

Table 1. Table showing the efficiency of wave propagation through a lattice of 5000 sites.

Dimensionless launch speed	Dimensional launch speed	Dimensional speed at end of lattice	Percentage difference
0.10	0.266	0.458	72.2%
0.20	0.531	0.861	62.1%
0.30	0.797	1.157	45.2%
0.40	1.062	1.466	38.0%
0.50	1.328	1.499	9.7%
0.60	1.593	1.629	2.3%
$\sqrt{\beta} \approx 0.71$	1.878	1.803	−4.0%
0.80	2.124	1.969	−07.3%
0.90	2.390	1.812	−24.2%
0.95	2.522	1.846	−26.8%

propagation of a solitary wave through the lattice is shown in figure 10, where the total number of lattice sites has been restricted to $N = 500$, and the time to $0 < t < 40$. In this figure it is possible to see a small amount of radiation emerge from the solitary wave at small times as the wave adjusts from the shape given by the initial conditions to a slightly different shape more appropriate to the discrete nature of the lattice. Following this the propagation of the wave through the lattice is remarkably clean, with very little radiation being shed at later times. Due to the periodic boundary conditions, small-amplitude linear waves leaving $n = 0$ travelling in the negative n direction reappear at $n = N$.

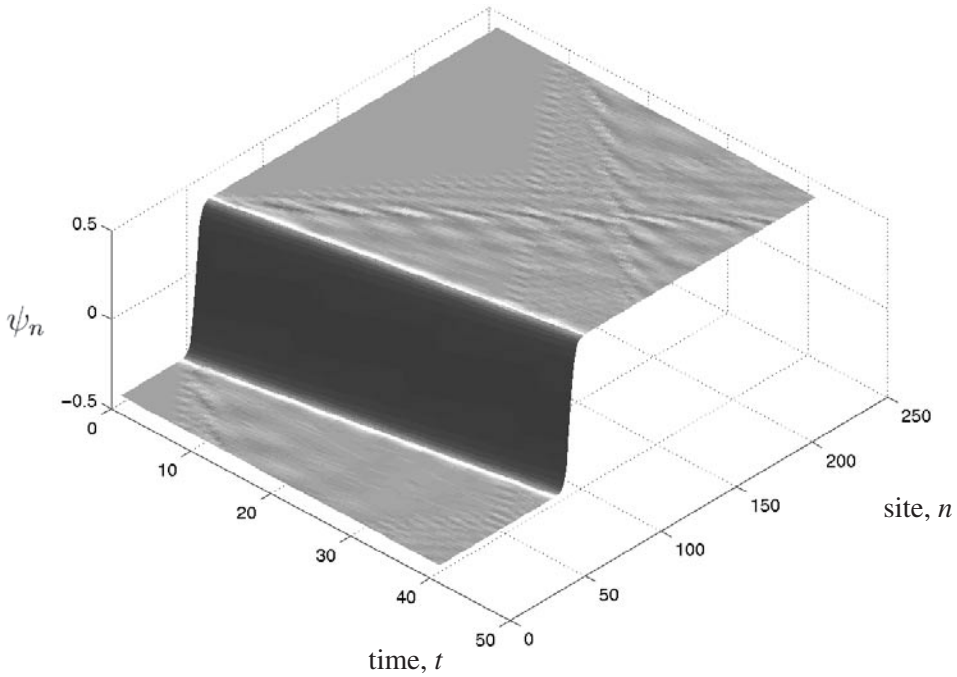

Figure 10. The propagation of a solitary wave through the sublattice of smaller atoms ($\psi_n(t)$). Note the small amount of radiation given off as the initial conditions adjust to the lattice, followed by the almost lossless propagation of the resulting modified wave through the lattice.

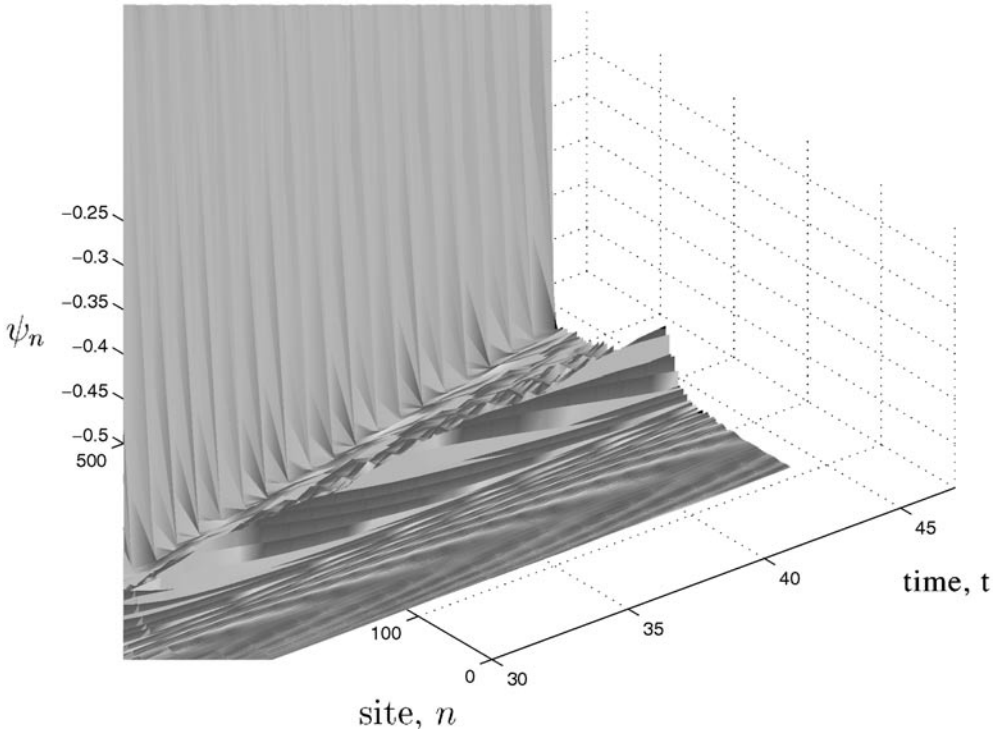

Figure 11. An enlargement of the tail of a solitary wave travelling at nondimensional speed of 0.9. The figure shows the effect on the sublattice of small atoms (ψ_n) for times $30 < t < 45$ and lattice sites $1 < n < 500$, and illustrates the small-amplitude radiation which is shed from the solitary wave as it travels through the lattice.

From the results presented in table 1, we see that slow waves are accelerated by the lattice, and fast waves are decelerated by the lattice. The speed of the wave thus appears to tend to an intermediate speed, which is approximately equal to the critical speed of $c_* = \sqrt{\beta}$. It should also be noted that the change in speed occurs slowly and gradually over a large period of time. Even after a time of 280 a wave initially travelling at a dimensional speed of 0.266 has only been accelerated to a speed of 0.458; it will thus take an extremely long time to approach the critical speed, which in this case is about 1.8. However, since the simulations initiated at larger speeds also show a convergence of speed over time to $\sqrt{\beta}$, we assume that given enough time and a large enough lattice a wave started at a speed of 0.266 will eventually be accelerated to 1.8. Thus, as well as making the analysis of travelling waves simpler, the special speed $c_* = \sqrt{\beta}$ seems to play an important physical role in the propagation of energy through the lattice.

Figure 11 shows that the propagation of the solitary wave through the lattice is not perfectly lossless, and is accompanied by a small amount of radiation. The initial speed in this case was chosen near the upper limit of allowable velocities to highlight the losses, as this is one of the more extreme cases. At speeds close to $\sqrt{\beta}$, the losses are less noticeable. A similar slow evolution of speed of a kink in a discrete system was noted in a detailed study by Peyrard and Kruskal [11] for the DSG system. In this monatomic system with only FNIs, the kink is slowed down, converging to a velocity of zero. The convergence was not simple, however, but has long periods of very slow reduction in speed, punctuated by faster reductions in speed

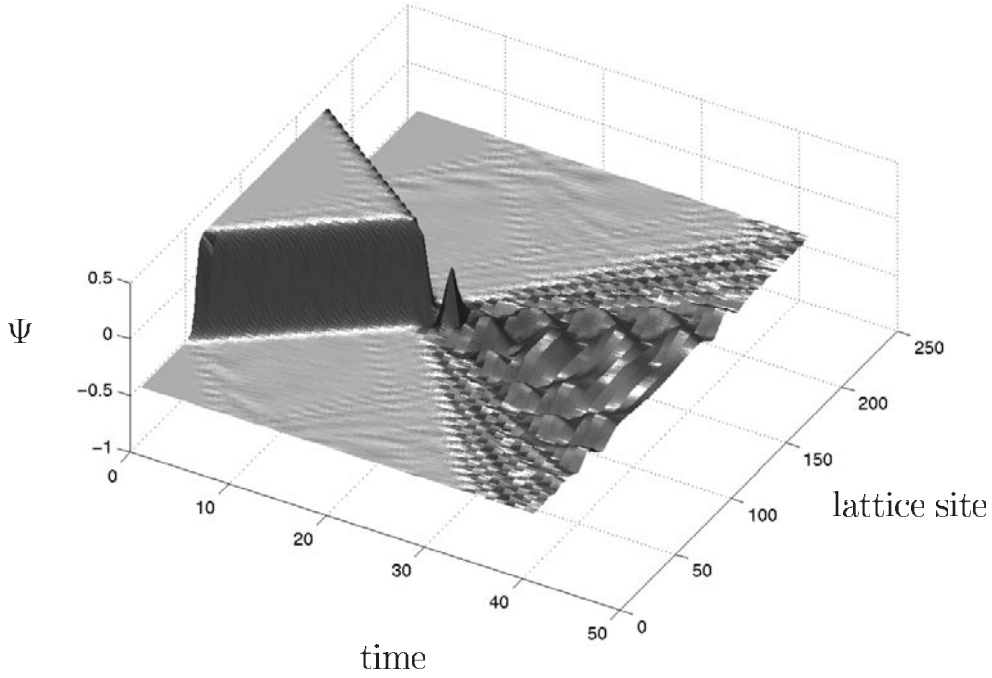

Figure 12. The collision between two solitary waves: displacements of the sublattice of small atoms (ψ_n). The near wave starts from the position $n = 100$, initially moving to the right at a dimensionless speed of $c = 0.4$, and the far wave starts at lattice site $n = 400$ and moves left (towards the reader), at a dimensionless speed of $c = -0.4$.

when the velocity coincides with certain well defined values independent of its launch velocity. These values correspond to wavenumbers where the frequency at which the kink passes over lattice sites matches the dispersion relation for small-amplitude linear waves. We expect a similar mechanism to hold for velocity changes of the kink in this more complicated lattice.

5.2. Collisions of solitary waves

Figure 12 illustrates the effect on the smaller atoms (that is, the $\psi_n(t)$ variables) of a collision between two solitary waves travelling in opposite directions but with the same speed. The system is thus symmetric, and in the example illustrated, the dimensionless speed was 0.4. The initial conditions are taken from the second-order quasi-continuum theory, (3.20), (3.21). As in the simulations described earlier, a small amount of radiation is emitted from the waves at small times as their shape is modified by the discrete structure of the lattice. At the collision the two waves annihilate each other producing a burst of radiation, which then spreads from the collision site to the whole lattice. Since the system is energy conserving, the energy dispersed is the same as the initial energy of the two solitary waves.

The effect of a nonsymmetric collision on the displacements of the larger atoms ($\phi_n(t)$) is illustrated in figure 13. In these variables the kink has a much smaller amplitude than in the $\psi_n(t)$ variables, with the consequence that the radiation emitted in this sublattice has a larger relative amplitude and is thus more noticeable. One solitary wave starts at the lattice site $n = 60$ and travels towards sites with larger numbers, initially at the extremely slow dimensionless speed of +0.01. As it progresses through lattice sites significant radiation is

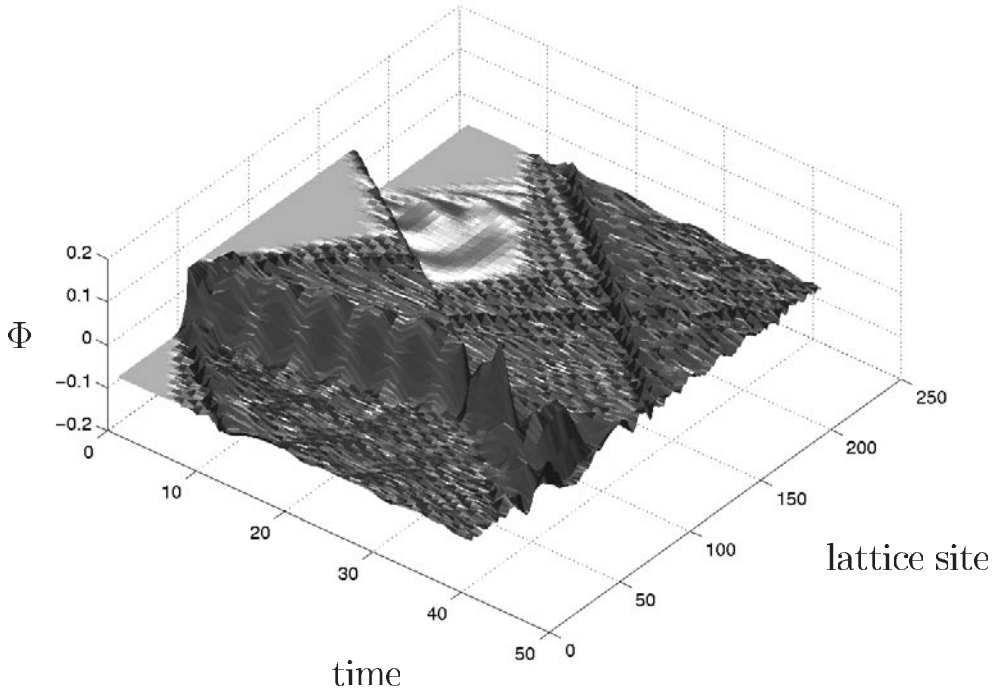

Figure 13. A collision between two kinks travelling in opposite directions and at different speeds: the displacements of the sublattice of larger atoms (ϕ_n). The near wave starts at lattice site $n = 60$ and travels to larger-numbered sites at a dimensionless speed of $c = +0.01$, and the second wave starts at lattice site $n = 175$ and at nondimensional speed of $c = -0.4$. The collision approximately occurs at site $n = 100$ and time $t = 30$.

generated and spread to the lattice both behind and in front of the kink; this is due to the effect of the Peierls–Nabarro potential. The second solitary wave starts at the lattice site $n = 174$ and travels at a nondimensional speed of -0.4 towards lattice sites of smaller number. A small amount of radiation can be seen to emerge from this wave as it initially adjusts its shape to the lattice. It is also apparent from figure 13 that the propagation of the second, faster wave is not affected by the noise generated by the first wave. The noise released from the slow wave passes through the fast wave with little effect, illustrating the stability and robustness of the wave. As in the symmetric collision illustrated in figure 12, the two solitary waves annihilate each other on impact and their energy is released and radiated to the lattice.

6. Discussion

This paper has introduced a new model for the study of diatomic lattices which include FNIs and SNIs together with on-site potentials for both the larger and smaller atoms. This is a modification of the models studied by Peyrard *et al* in [12] and [5], and Henry and Oitmaa [9]. Our model exhibits two types of equilibrium solution. If the FNIs are sufficiently attractive then the lowest-energy state of the chain has the atoms equally spaced. However, the more interesting scenario occurs when the on-site potential for the small atoms is dominant and at lowest energy each small atom lies close to one of the neighbouring larger atoms. There are then two equal-energy ground states: one where all small atoms are closer to the larger atom

on their left, and a second state where they lie closer to the right large atom. Following the quench of such a chain, one expects to find regions in which all smaller atoms occupy the same state, and smaller regions (domain walls) where a transition between the two states occurs. Thus the main body of this paper addresses systems in which one ground state is approached at one end of a chain in the lattice, and the other ground state at the other end of the chain. Such transition regions are modelled as solitary waves (kinks) and the remainder of the paper addresses the shape and mobility of these waves.

The majority of existing quasi-continuum techniques have been limited by their ability to predict the shape of the solitary wave only for one special speed of propagation through the lattice. This is caused by the equations of motion yielding two coupled sets of equations: one for the smaller atoms and a second for the larger atoms; only at one special speed do they decouple. One purpose of this paper is to generalize quasi-continuum techniques so that solutions of arbitrary speed can be found; we have achieved this by showing how to decouple the system of equations, so that at arbitrary speeds the solution in the sublattice of smaller atoms can be solved, and then used to find the solution for the larger atoms. Similar results have been obtained by Henry and Oitmaa on a simpler lattice [9]. Applying second-order quasi-continuum theory to the discrete system for general speeds, we derived analytical approximations for *kink*-type solutions. Our results show that faster waves are narrower than slower waves. The analytic form shows that there is a maximum speed for kinks, though this is not the same as the special speed for which the previously available continuum theory gave a solution.

We then extended the continuum theory to include fourth-order derivatives. Quasi-continuum theory was again applied and Padé approximations used to derive travelling wave solutions for a range of speeds. On plotting these solutions and comparing them with those correct to second order, we discovered that the higher-order solutions have a slightly smaller width than the second-order solutions derived earlier. The analytical results give an indication of why fast waves do not propagate through the lattice. At larger speeds, the wave in the sublattice of larger atoms develops large oscillations, see figures 7 and 9. While both approximations show oscillations in the shape of the kink, two types of oscillation are observed: in the second-order theory (figure 7) the oscillation is centred on the unstable zero-equilibrium solution, whereas the fourth-order solution (figure 9) exhibits an additional oscillation around the stable equilibrium solution $\Psi = \pm\tilde{\Psi}$ before crossing the unstable zero solution.

Extensive numerical simulations of the discrete system confirmed the quasi-continuum theory to be accurate and that a kink propagates well when launched at a variety of speeds from small, through the special speed ($c_c = \sqrt{\beta}$) identified in the previous continuum theory, up to the maximum speed found in our theory. Thus our model differs from the model studied by Peyrard *et al* [12], in which waves initiated at a speed faster than the special speed do not propagate through the lattice. However, over long time simulations it appeared from our results that waves prefer to travel at this special speed (c_c). The waves adjust to this speed by the emission of radiation; we expect this loss of energy to be due to the Peierls–Nabarro potential of the lattice. This speed was identified as being special in the analytical work as the speed which mathematically greatly simplifies the system. We suggest that at this speed the lattice also experiences a minimum stress due to the wave. Note that this includes the counter-intuitive behaviour of waves losing energy by speeding up; a similar phenomenon has been observed previously in a lattice with SNIs [18], where slower waves actually carry more energy than faster ones.

We were also able to investigate how waves interact with each other in collisions—which cannot be deduced analytically. The collision of a kink with an antikink travelling in the opposite direction leads to the destruction of both waves, the energy of both waves being

emitted as radiation. At the start of the simulation, the solitary wave adjusted its shape very slightly from the continuum approximation used as initial conditions to the shape appropriate for the discrete lattice. This adjustment results in the emission of a small amount of radiation, which the kink then travels over, without any obvious change in shape or speed. Thus the kinks appear to be stable and robust to noise in the system.

Open questions remain for the lattice we have studied here, for example we have not tackled the existence of breathers, either stationary or moving; nor have we attempted the extremely delicate numerical tests needed to find the size and shape of the Peierls–Nabarro potential for the system.

References

[1] Benjamin T B, Bona J L and Mahoney J J 1972 Model equations for long waves in nonlinear dispersive systems *Phil. Trans. R. Soc.* **272** 47–78

[2] Collins M A 1981 A quasi-continuum approximation for solitons in an atomic chain *Chem. Phys. Lett.* **72** 342–7

[3] Collins M A 1983 Solitons in chemical physics *Adv. Chem.* **53** 225–340

[4] Collins M A and Rice S A 1982 Some properties of large amplitude motion in an anharmonic chain with nearest neighbour interactions *J. Chem. Phys.* **77** 2607–22

[5] Cretegny T and Peyrard M 1996 Collective coordinate treatment of discreteness effects in hydrogen-bonded chains *Phys. Lett.* A **210** 347–58

[6] Duncan D B, Eilbeck J C, Feddersen H and Wattis J A D 1993 Solitons on lattices *Physica* D **68** 1–11

[7] Duncan D B, Eilbeck J C, Walshaw C H and Zakharov V 1991 Solitary waves on a strongly anisotropic KP lattice *Phys. Lett.* A **158** 107–11

[8] Fermi E, Pasta J R and Ulam S 1955 *Los Alamos Scientific Laboratory Report* LA-1940

[9] Henry B I and Oitmaa J 1985 Dynamics of a nonlinear chain II thermodynamic properties *Aust. J. Phys.* **38** 171–89

[10] Kofane T, Michaux B and Remoissenet M 1988 Theoretical and experimental studies of diatomic lattice solitons using an electrical transmission line *J. Phys. C: Solid State Phys.* **21** 1395–412

[11] Peyrard M and Kruskal M D 1984 Kink dynamics of the highly discrete sine–Gordon system *Physica* D **14** 88–102

[12] Peyrard M, Pnevmatikos S and Flytzanis N 1987 Dynamics of two-component solitary waves in hydrogen-bonded chains *Phys. Rev.* A **36** 903–14

[13] Pnevmatikos S, Flytzanis N and Remoissenet M 1986 Soliton dynamics of nonlinear diatomic lattices *Phys. Rev.* B **33** 2308–21

[14] Pnevmatikos S, Remoissenet M and Flytzanis N 1983 Propagation of acoustic and optical solitons in nonlinear diatomic chains *J. Phys. C: Solid State Phys.* **16** L305–10

[15] Remoissenet M 1994 *Waves called Solitons: Concepts and Experiments* (Berlin: Springer)

[16] Rosenau P 1986 Dynamics of nonlinear mass spring chains near the continuum limit *Phys. Lett.* A **118** 222–7

[17] Wattis J A D 1992 Approximations to solitary waves on lattices: II. Quasi-continuum methods for fast and slow waves *J. Phys. A: Math. Gen.* **26** 1193–209

[18] Wattis J A D 1996 Approximations to solitary waves on lattices: III. The monatomic lattice with second-neighbour interactions *J. Phys. A: Math. Gen.* **29** 8139–57

[19] Wattis J A D 1994 Solitary waves on a two-dimensional lattice *Phys. Scr.* **50** 238–42

[20] Wattis J A D 1998 Stationary breather modes of generalised nonlinear Klein–Gordon lattices *J. Phys. A: Math. Gen.* **31** 3301–23

[21] Wattis J A D 2001 Quasi-continuum approximations for diatomic lattices *Phys. Lett.* A **284** 16–22

[22] Zabusky N and Kruskal M 1965 Interactions of solitons in a collisionless plasma and the recurrence of initial states *Phys. Rev. Lett.* **15** 240–3